The Journal of Chemical Physics ARTICLE scitation.org/journal/jcp

Effect of fine-tuning pore structures on the dynamics of confined water

Cite as: J. Chem. Phys. 150, 204706 (2019); doi: 10.1063/1.5096771
Submitted: 19 March 2019 • Accepted: 3 May 2019 •
Published Online: 28 May 2019

A. I. Kolesnikov,[1,a)] L. M. Anovitz,[2] F. C. Hawthorne,[3] A. Podlesnyak,[1] and G. K. Schenter[4]

AFFILIATIONS

[1]Neutron Scattering Division, Oak Ridge National Laboratory, Oak Ridge, Tennessee 37831, USA
[2]Chemical Sciences Division, Oak Ridge National Laboratory, Oak Ridge, Tennessee 37831, USA
[3]Department of Geological Sciences, University of Manitoba, Winnipeg, Manitoba R3T 2N2, Canada
[4]Physical Sciences Division, Pacific Northwest National Laboratory, Richland, Washington 93352, USA

Note: This paper is part of a JCP Special Topic on Chemical Physics of Supercooled Water.
[a)]**Author to whom correspondence should be addressed:** kolesnikovai@ornl.gov

ABSTRACT

Confinement of water in sub-nanometer pores strongly alters its vibrational dynamics from that of bulk water. The effect of confinement can, furthermore, be finely tuned by small changes in the size and symmetry of the confining pore. Using inelastic neutron scattering (INS), we recently studied the dynamics of water confined in the channels of beryl and cordierite in which, at low temperatures, water shows similar behavior, indicating an absence of hydrogen bonds acting on the water molecule and a shallow water potential in the direction perpendicular to the channels. In addition, we observed multiple tunneling modes (between 0.66 and 14.7 meV) in the INS spectra of beryl due to transitions between the split ground-state of the water protons. Here, we present a study of (i) the effect of pressure on the dynamics of water in beryl, (ii) the dynamics of water in beryl containing alkali metals (which results in changing the orientation of the water molecule in the crystal), and (iii) the dynamics of water in cordierite at low energies. We found a shift in the tunneling and vibrational modes of water in beryl to higher energies at 22 kbar relative to 1 bar. No tunneling modes were observed for water in cordierite and type-II water in beryl. Therefore, we conclude that very small differences in the size and structure of the pores and the orientation of the water molecule in these minerals result in changes in the potential of the water protons and drastic changes in the confined water dynamics.

I. INTRODUCTION

The vibrational dynamics of confined water differs strongly from that of bulk water, although the extent of the change depends on the size and shape of the confining pores. Of particular interest is water confined in hydrophobic pores, e.g., in single-wall carbon nanotubes (SWNTs) and fullerenes, where water interacts only weakly with the surface of the pore and displays significant quantum behavior. Inelastic neutron scattering (INS) is a very powerful technique for studying the dynamics of water (as bulk and in confinement) due to the very large neutron-scattering cross section of hydrogen compared to other atoms. Because of this factor, INS spectra mostly contain information on the dynamics of water protons. For example, INS showed that water encapsulated in fullerene C_{60} exhibits quantum transitions between the para and ortho states,[1,2] and water in ~14 Å diameter SWNTs shows anomalously soft dynamics.[3] Molecular dynamics (MD) calculations for water in 13.8 Å diameter (10, 10) SWNTs suggested a new structure for nanotube water[3] consisting of a square-ice sheet wrapped into a cylinder in the nanotube (shell water) with interior molecules in a chainlike configuration. The soft dynamics of nanotube-water arises mainly from the drastic change in hydrogen-bond connectivity of the central chain water, which results in frequent breaking and forming of hydrogen bonds between the water molecules in the chain and the shell–chain molecules. The MD simulations for water in (9, 9) SWNTs of smaller diameter (~12.5 Å) suggested a nanotube-water structure composed only of shell water, which does not show the pliable water dynamics of the first configuration.[4] Thus, both INS measurements and MD

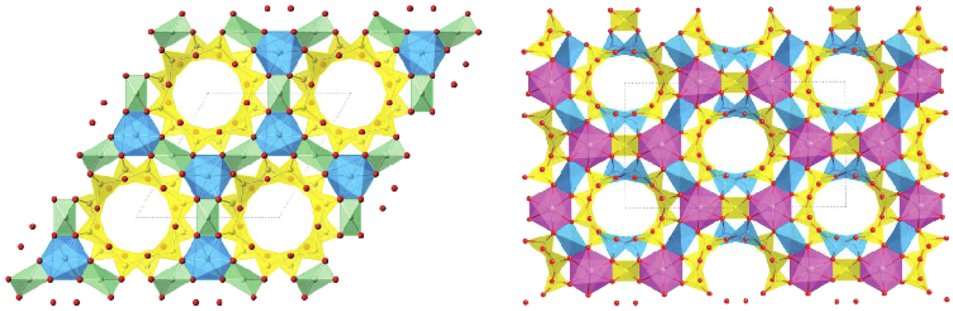

FIG. 1. The crystal structures of beryl $Be_3Al_2Si_6O_{18}$ (left) and cordierite $Al_4Mg_2Si_5O_{18}$ (right) showing large open channels running parallel to the crystallographic *c*-axis (looking down the *c*-axis). The channels consist of six-membered rings of SiO_4 tetrahedra (yellow) in beryl and four SiO_4 (yellow) and two AlO_4 tetrahedra (blue) in cordierite. The rings are cross-linked by BeO_4 tetrahedra (green) and AlO_6 octahedra (blue) in beryl, and by AlO_4 tetrahedra (blue) and MgO_6 octahedra (pink) in cordierite. Type-I water molecules occupy positions in the center of the channels and have their H–H axis parallel to the *c*-axis of each structure. The dimensions of the unit cells are a = 9.21 Å and c = 9.19 Å for beryl[8] (space group *P*6/*mcc*) and a = 17.08 Å, b = 9.72 Å, and c = 9.34 Å for cordierite[9] (space group *Cccm*).

simulations suggest that the dynamics of quasi-one-dimensional nanotube water is very sensitive to the geometry of the confining pore: changing the radius of SWNTs by a fraction of an angstrom is sufficient to switch on and off the channeling of water molecules along the nanotube.

Recently, we used INS to study[5–7] the dynamics of water in single crystals of beryl and cordierite, in which water is confined in channels of approximately 5 Å diameter. Beryl is hexagonal (space group *P*6/*mcc*), with channels along the *c*-axis bounded by six-membered rings of SiO_4 tetrahedra (see Fig. 1, left).[8] Cordierite has a similar structure but is orthorhombic (space group *Cccm*), with a six-ring channel along the *c*-axis made of four SiO_4 and two AlO_4 tetrahedra, which causes the reduction in symmetry and forces the rings to become somewhat elongated (Fig. 1, right).[9] The channels in beryl and cordierite form cavities (which may contain water or alkali cations) about 5.1 and 5.5 Å in diameter, respectively, separated by narrow (~2.8 Å) "bottlenecks" which prevent direct contact between water molecules along the channel. In the case of our previous work,[5–7] both crystals were low-alkali samples, in which water has its H-H axis parallel to the *c*-axis of the crystal (type-I water), and, in the case of beryl, water protons were distributed over the 6-fold equivalent positions across the channels, above and below the oxygen site. Note that, in alkali-rich beryl, the water orientation changes to type-II water in which the H-H axis lies in the *ab*-plane of the crystal and its dipole moment lies along the *c*-axis.

At a low temperature, the INS spectra[5–7] for both samples at large energy transfer show intramolecular O-H stretching modes at ~465 meV and the H-O-H bending (or scissor) mode at 197.5 meV, which correspond to the values for a water molecule in the gas state with no hydrogen bonds (HBs) acting on the water. The intensities of these stretching and bending modes are strong along the *c*-axis and weak in the perpendicular direction. In addition, the spectra obtained with a large incident neutron energy (E_i = 800 meV) show a behavior similar to neutron-recoil scattering on an atom of 1 a.u. mass for momentum transfer in the *ab*-plane, confirming a model of a shallow rotational potential for water protons in beryl and cordierite across the channel. Another INS study[10] of beryl showed multiple peaks at 0.66, 1.49, 1.63, 7.9, 8.4, 12.7, and 14.7 meV which were assigned to transitions between split levels of the ground state of water protons due to their tunneling between the 6-fold positions across the channel. The intensities of these tunneling peaks strongly decrease with increasing temperature (due to temperature depopulation of the lower split ground-state). The intensities increase as a function of neutron momentum transfer, which corresponds with the known form-factor for water proton jumps between the 6-fold positions and proves that the observed transitions are not magnetic in origin. Quantum tunneling of water was suggested before to explain the fine structure of the optical spectra of beryl.[11–13] Deep inelastic neutron scattering[10,7] and density functional theory (DFT) calculations[10] further confirm water tunneling in beryl at a low temperature.

In the current work, we present an INS study of water (type-I) in beryl under pressure to investigate changes in the dynamics of the ultraconfined water due to contraction of the channels. We also compare the INS spectra for beryl with type-II water with that of type-I water in beryl and compare both to the INS spectra of cordierite, in which water has a slightly different confinement geometry. This comparison allows us to evaluate the effects of relatively small changes in confinement size and structure on the dynamics and tunneling behavior of water.

II. METHODS

A. Experimental details

Gem-quality single crystals of beryl ($Be_3Al_2Si_6O_{18}$) with type-I and type-II water, and cordierite ($Al_4Mg_2Si_5O_{18}$) with type-I water, all containing about 2 wt. % H_2O water, were used in the INS experiments reported here. The first was gem rough from Pakistan, the second was from the Tanco pegmatite,[14] and the third was gem rough of unknown origin. We also measured the spectra for dehydrated cordierite, which was produced from cordierite by exposing it at 1100 °C in rough vacuum for about 10 h. The single-crystal beryl with type-I water was powdered for high-pressure INS measurements and for measurements at ambient pressure as a control. The single crystals of beryl with type-II water and cordierite were cut into flat slabs approximately 0.7 mm thick to reduce multiple scattering.

For *in situ* high-pressure experiments, we used a clamp piston-cylinder Ni-Cr-Al pressure cell,[15] with an inner diameter of 4.8 mm, an outer diameter 18 mm, and an effective sample volume of ~0.3 cm^3. The powdered beryl sample was mixed with Fluorinert liquid (used as pressure-transmitting medium) and pressurized to 22 kbar. To quantify the background signal from the pressure cell, INS spectra were also measured for the pressure cell filled with Fluorinert liquid without the beryl sample at ambient pressure and the same temperature and incident neutron energies.

The INS measurements were done using the time-of-flight direct geometry spectrometers SEQUOIA[16,17] and CNCS[17–19] at the Spallation Neutron Source (SNS) at the Oak Ridge National Laboratory. To provide high energy resolution, about 1%–5% of the incident neutron energy (E_i), in a wide range of energy transfer values ($E < 550$ meV), the data were collected with different E_i values ranging from 12 to 800 meV. The neutron momentum transfer (Q) range covered in the experiments was between 0 and 17 $Å^{-1}$, depending on E_i, energy transfer, and the scattering angle. The measurements were done at different temperatures (T) using a bottom-loading closed-cycle helium refrigerator (T_{min} = 5 K) and a top-loading helium-flow cryostat (T_{min} = 1.7 K). The INS data were corrected for detector efficiency and transformed from time-of-flight and instrument coordinates to the dynamic structure factor $S(Q, E)$ with the MANTIDPLOT[20] and DAVE[21] software packages for data reduction and analysis. In one-phonon approximation, the measured neutron energy-loss $S(Q, E)$ spectrum relates to the partial generalized phonon density of states $G_i(E)$ as[22]

$$S(Q,E) = \frac{\hbar^2 Q^2}{6E} \sum_i \frac{\sigma_i^t}{m_i} e^{-2W_i(Q)} G_i(E)[n(E,T)+1], \qquad (1)$$

where the sum is over all atoms in the crystal unit cell; $n(E, T) = 1/[\exp(E/k_BT) - 1]$ is the population Bose factor; σ_i^t, m_i, and $W_i(Q) = \langle u_i^2 \rangle Q^2/2$ are the total neutron-scattering cross section, mass, and Debye-Waller factor for atom i; and $\langle u_i^2 \rangle$ is the mean-squared displacement of atom i. Hydrogen has mostly incoherent neutron scattering (σ_H^{inc} = 80.26 barn and σ_H^{coh} = 1.7568 barn), and all other atoms in the minerals have predominantly coherent cross sections. The total neutron-scattering cross sections can be used in Eq. (1) because for averaged $S(E, Q)$, summed over large covered Q-range, the incoherent approximation for coherent-scattering materials is well justified.[23] Due to the small atomic mass and much larger neutron-scattering cross section for hydrogen (σ_H = 82.02 barn, compared to σ_{Be} = 7.63 barn, σ_{Al} = 1.503 barn, σ_{Si} = 2.167 barn, σ_O = 4.232 barn, and σ_{Mg} = 3.71 barn, see Ref. 24), the signal in the INS spectra is determined mainly by scattering from hydrogen atoms.

B. Computational details

The DFT electronic structure calculations were done using a 119 atom supercell, $4(Al_4Mg_2Si_5O_{18})$, with dimensions 17.071 Å, 9.715 Å, and 9.344 Å. The calculations were done using the Quickstep module of the CP2K software and periodic boundary conditions, and a 600 Ry cutoff was used for the density grid in CP2K.[25] The valence electrons were treated explicitly at the DFT level using the Perdew-Burke-Ernzerhof (PBE) functional.[26] A DZVP MOLOPT basis set[27] was used, and the core electrons on all atoms were represented by Goedecker-Teter-Hutter (GTH) pseudopotentials.[28]

III. RESULTS AND DISCUSSION

A. Effect of high pressure

Figure 2 shows the $S(E, \Delta Q)$ spectra obtained from $S(Q, E)$ data by summation over accessible Q-range (ΔQ) for beryl powder at 22 kbar and 1.7 K measured with E_i = 12 and 25 meV on the SEQUOIA spectrometer. The spectra are compared to those at ambient pressure measured with E_i = 12 meV (T = 6 K, single crystal, $\mathbf{Q} \perp c$-axis, SEQUOIA) and 28 meV (T = 1.7 K, powder, CNCS spectrometer). At 22 kbar, the tunneling peaks for water in beryl shift to higher energies −8.55, 12.87, and 15.01 meV compared to 8.3, 12.6, and 14.75 meV for ambient-pressure powdered beryl. Spectra measured with higher energy resolution (E_i = 12 meV) resolve a splitting of the ~8.5 meV peak into two peaks at 8.15 and 8.6 meV at 22 kbar, compared to 7.9 and 8.4 meV at ambient pressure, and a peak due to water translational vibrations along the c-axis shifts from 10.75 meV at ambient pressure to 11.06 meV at 22 kbar. The relative shift of all these peaks ($\Delta E/E$) is about 2.5%. The volume of the beryl unit-cell at room temperature contracts by V_P/V_0 = 0.987 upon applying a pressure of 24.1 kbar[29] (with contraction of a and c unit cell parameters by a_P/a_0 = 0.9963 and c_P/c_0 = 0.9947, respectively), with a larger contraction along the c-axis than along the a-axis (c/a = 0.9991 at 24.1 kbar, compared to 1.0007 at ambient pressure). The observed shift in the translational peak to higher energy is therefore due to an increase in the stiffness of the water vibration potential along the c-axis due to shortening of the water-to-cage distances in that

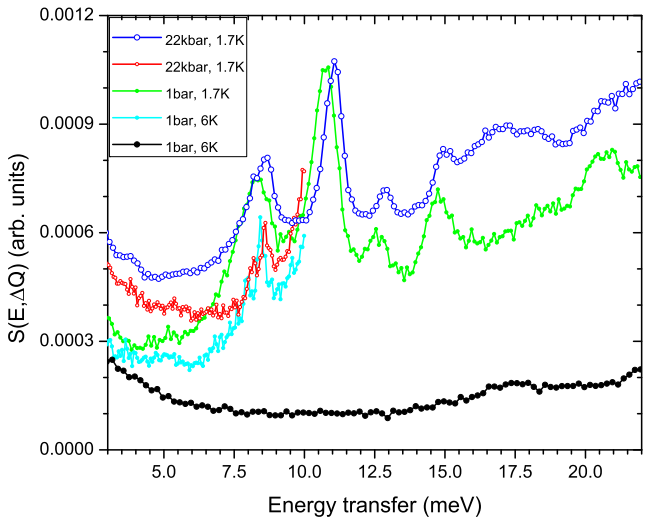

FIG. 2. $S(E, \Delta Q)$ spectra of powdered beryl at 22 kbar and 1.7 K measured with E_i = 12 and 25 meV compared to those at ambient pressure measured with E_i = 12 meV (T = 6 K, single crystal, $\mathbf{Q} \perp c$-axis) and 28 meV (T = 1.7 K, powder). The spectra obtained with E_i = 12 and 25 meV were collected at SEQUOIA and with E_i = 28 meV at CNCS. The black curve at the bottom is the spectrum of the high-pressure cell filled with Fluorinert liquid without the sample, measured with E_i = 25 meV at T = 6 K at SEQUOIA.

direction. Shifts in the tunneling peaks to higher energies imply an increase in the splitting energies of the ground state of the water protons. The tunneling splitting of the ground state for a particle (in our case hydrogen) of mass m in the double-well potential $U(x)$ can be calculated by the expression[30]

$$E_t^{calc} = {}^{E_1}/_{\pi} \exp\left(-{}^{1}/_{\hbar} \int \sqrt{2m[U(x) - E_G]}\,dx \right), \quad (2)$$

where E_G and E_1 are the energy of the hydrogen ground-state and vibrational mode, respectively, in the direction of tunneling, and the integral should be taken under the barrier between the turning points of the hydrogen. Therefore, the barrier height of the potential for water rotation around the c-axis decreases. Similar behavior was observed recently for hydrogen tunneling in α-Mn,[31] where application of pressure (up to 30 kbar) results in shift of the tunneling peak to higher energies due to a decrease in the height of the potential barrier.

In addition to the shifts noted above, a feature (a broad peak) appears at around 17 meV in the 22 kbar beryl spectrum that is not present at ambient pressure. This broad peak could be due to librational vibrations of the water molecule around the c-axis (which is around 20 meV in the ambient pressure spectrum), which appear at lower energy at high pressure due to softening of the potential for water rotation in the ab-plane.

B. Dynamics of type-II water in beryl

INS spectra of a beryl single crystal with type-II water were first measured with E_i = 800 meV and the neutron momentum transfer (**Q**) oriented both parallel and perpendicular to the c-axis. As in the spectra of beryl and cordierite with type-I water,[5–7] the spectra for type-II water in beryl show high energy values for the intramolecular O-H stretching modes (~465 meV), indicating an absence of hydrogen bonds acting on the water molecules. Figure 3 shows a contour plot of the difference in $S(Q, E)$ between spectra measured with **Q** perpendicular and parallel to the c-axis. This indicates a significant amount of extra intensity close to the calculated neutron-recoil line for scattering from free protons, $E_R = \hbar^2 Q^2/2m$. As discussed in our previous papers,[5–7] this recoil-like behavior indicates a softer "effective" potential for water protons perpendicular to the c-axis. Therefore, regardless of the orientation of the water molecule in the channel (type-I or type-II water), the potential for water protons in beryl and cordierite across the channel is softer than along the c-axis.

The $G(E)$ spectra obtained from INS data measured with E_i = 250 meV (Fig. 4) show an intramolecular H-O-H bending-mode peak for water at 202.7 meV. This peak is strong for the **Q**||c-axis and weak for the **Q**⊥c-axis. Satellite peaks occur in the

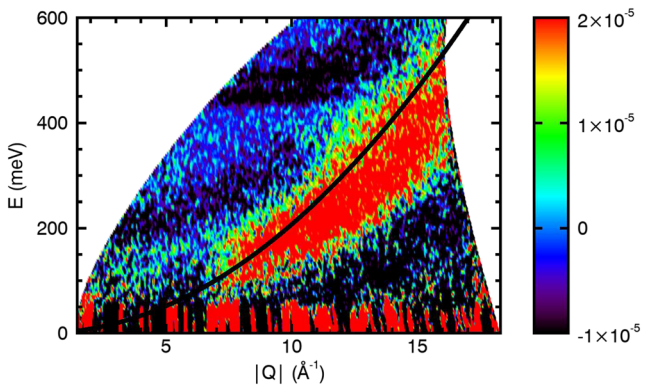

FIG. 3. $S(Q, E)$ contour plot showing the difference between the data collected for beryl with type-II water with **Q** perpendicular and parallel to the crystal c-axis. These spectra were measured with E_i = 800 meV at T = 5 K. The solid black line shows the scattering behavior of neutrons on free protons.

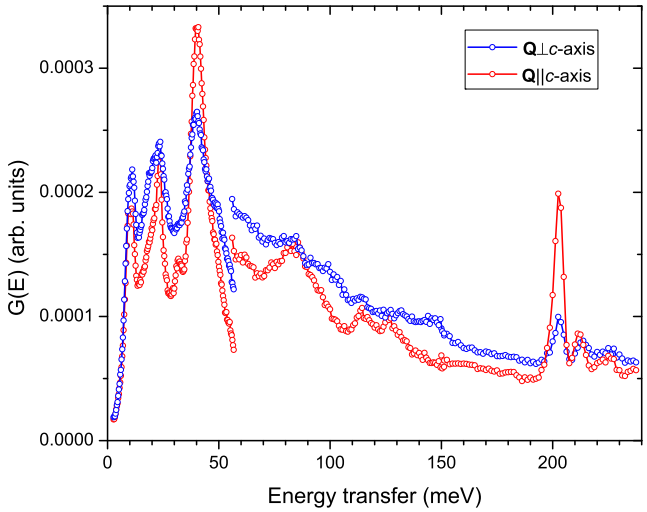

FIG. 4. $G(E)$ spectra for beryl with type-II water measured with E_i = 60, 160, and 250 meV (merged data) and **Q** parallel and perpendicular to the crystal c-axis at T = 5 K.

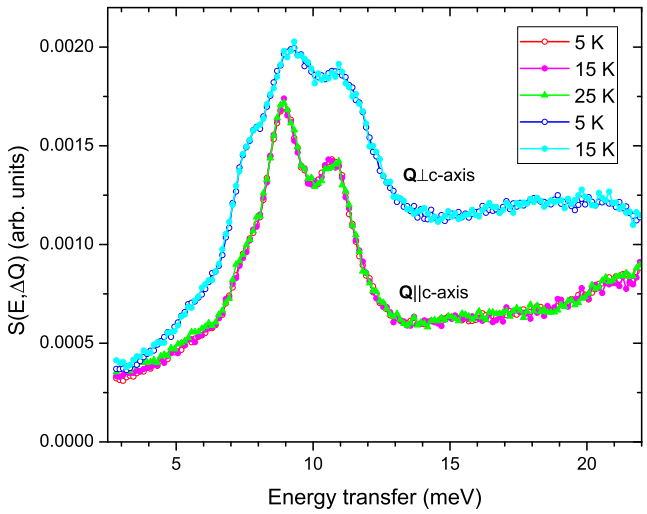

FIG. 5. $S(E, \Delta Q)$ spectra for beryl with type-II water measured with E_i = 25 meV and **Q** parallel and perpendicular to the c-axis of the crystal at different temperatures.

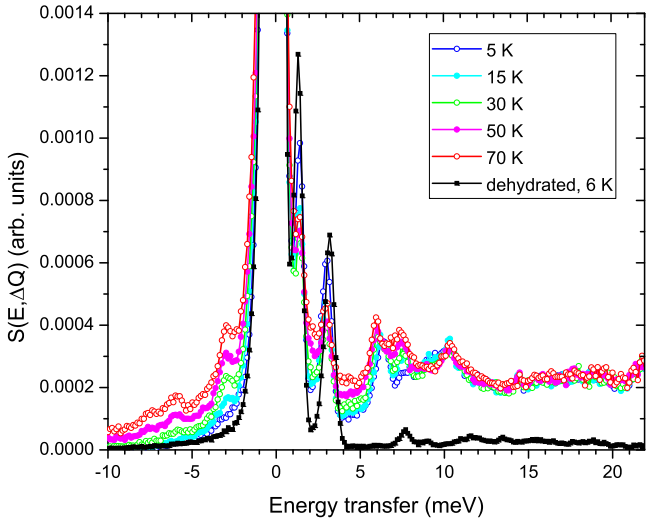

FIG. 6. The dynamical structure factor $S(E, \Delta Q)$, summed over $Q = 0.4–3.1$ Å^{-1}, for single-crystal cordierite (with $\mathbf{Q}\perp c$-axis), measured with $E_i = 25$ meV at different temperatures. The spectrum of powdered dehydrated cordierite (black curve) is also shown for comparison.

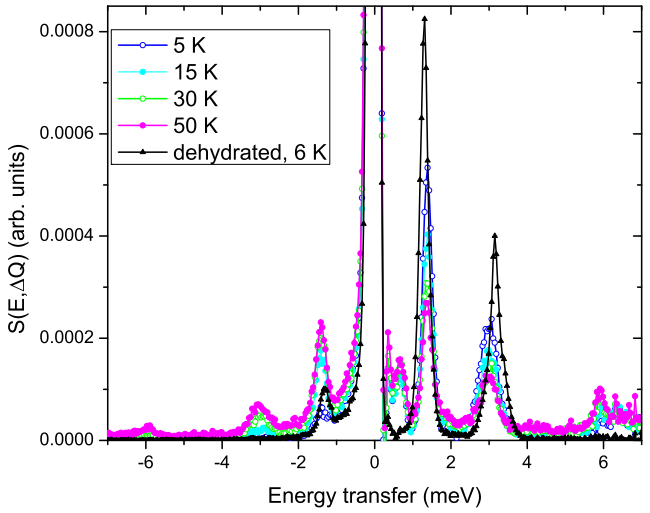

FIG. 7. The dynamical structure factor $S(E, \Delta Q)$, summed over $Q = 0.3–1.7$ Å^{-1}, for single-crystal cordierite (with $\mathbf{Q}\perp c$-axis) and powdered dehydrated cordierite, measured with $E_i = 8$ meV at different temperatures.

spectra for the $\mathbf{Q}||c$-axis at 211.8 and 224 meV (shifted from the main peak by about 9 and 21 meV, respectively) and for $\mathbf{Q}\perp c$-axis at 213.5 and 225 meV (shifted by about 11 and 22 meV, respectively). These can be related to two- and three-phonon neutron-scattering involving a combination of the intramolecular bending mode (202.7 meV), low-energy intermolecular translational modes at 9 and 10.8 meV (see Fig. 5), and bending and librational modes around 22 meV.

Several other peaks are observed in these spectra. Two strong peaks at ~22 and 40 meV can be assigned to librational modes. However, the peak at 40 meV is probably a superposition of the 40 meV librational mode and two-phonon neutron scattering of the 22 meV librational mode. In addition, the broad peak at about 82 meV is possibly due to two-phonon neutron scattering of the 40 meV librational mode.

Figure 5 shows the low-energy part of the $S(E, \Delta Q)$ spectra, which are due to translational vibrations of water molecules. These vibrational bands have two maxima at about 9 meV (with a low-energy shoulder at ~7.8 meV) and 10.8 meV. The intensity of the band is larger for measurements where $\mathbf{Q}\perp c$-axis than where $\mathbf{Q}||c$-axis. This extra intensity at low energies implies that the mean-squared displacement of water protons in the *ab*-plane is larger than that along the *c*-axis. As a result, the Debye-Waller factor strongly suppresses the INS intensity of the intramolecular modes around 202 and 465 meV for $\mathbf{Q}\perp c$-axis measurements.[5]

As temperature increases from 5 to 15–25 K, the intensities of the peaks in the spectra measured with $E_i = 25$ meV change very little, in contrast to what was observed for type-I water in beryl.[10] This means that type-II water in beryl shows no evidence of tunneling behavior, although it still exhibits significant mobility in the *ab*-plane, which is comparable to that observed in type-I water in beryl.

C. Dynamics of water in cordierite

Figures 6 and 7 show the INS spectra of cordierite measured with $E_i = 25$ and 8 meV at temperatures between 5 and 70 K. The intensities of the peaks at 1.4 and 3.0 meV significantly decrease with increasing temperature. This implies that these peaks are not due to vibrational excitations but due to transitions between split levels of the ground state. The figures also show the spectra for dehydrated cordierite, which displays similar peaks, but at slightly

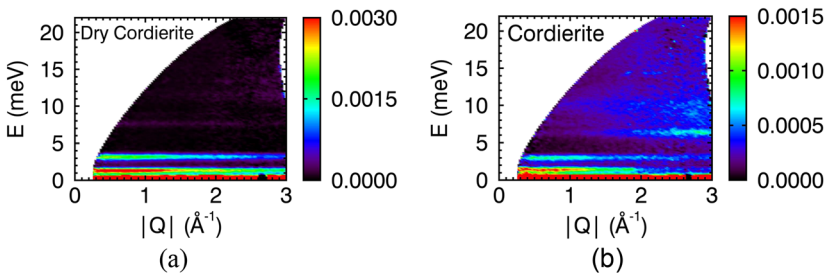

FIG. 8. Contour plot of the dynamical structure factor $S(Q, E)$ for single-crystal cordierite ($\mathbf{Q}\perp c$-axis and $T = 5$ K) and powdered dehydrated cordierite ($T = 6$ K), measured with $E_i = 25$ meV.

different positions (1.3 and 3.15 meV). This proves that the origin of these peaks cannot be related to water. The contour plots of $S(Q, E)$ for cordierite and dehydrated cordierite measured with E_i = 25 meV at 5 and 6 K, respectively, are shown in Fig. 8. These show that the intensities of these peaks decrease with increasing neutron-momentum transfer (Q). Thus, they are of magnetic origin.[10] As natural cordierite is expected to contain some ferrous ion substituting for magnesium[32] this is not unexpected. Earlier work[33] reported similar peaks in the INS spectra of cordierite. These were explained as transitions between a split ground state caused by the crystal electric field experienced by $^{(6)}Fe^{2+}$ in the structure, and are in accord with the present data. The INS spectra of dehydrated cordierite also show another weak peak at 7.7 meV, the intensity of which also decreases with increasing momentum transfer, similar to the dependence observed for the peaks at 1.3 and 3.15 meV (Fig. 9).

At low energies, the INS spectra of cordierite show two translational vibrations of the water molecule at ~6 and 10.5 meV, in agreement with previous INS studies.[34,6] However, at energies between 5 and 8 meV, the spectrum shows unusual thermal behavior. At T = 5 K, there is a peak at 6.4 meV (Fig. 10). At 15 K, a shoulder appears at the left side of this peak and grows in intensity at higher temperatures into a sharp peak at 5.9 meV. Figure 11 shows the spectra in this energy range as generalized vibrational density-of-states, $G(E)$, in which the data are corrected for the thermal population factor [see Eq. (1)]. Hence, presented in this manner, the vibrational spectra should not be sensitive to temperature (if the Debye-Waller factor is ignored). Therefore, the observation that with an increase in temperature there is a strong drop in intensity at 6.4 meV (the peak disappears at 50 K) and a fast-growing sharp peak at 5.9 meV (the peak reaches its maximum value at 30 K and does not change at higher temperatures) indicates a possible phase transition between 15 and 30 K. Most likely, this suggests that, at a temperature around 20 K, there is a slight change in the position of water in the cordierite channel, but low-temperature neutron diffraction data are needed to confirm this conclusion.

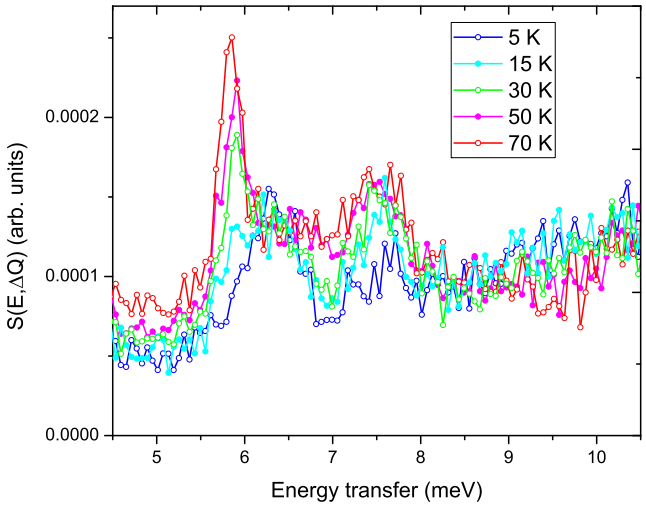

FIG. 10. The dynamical structure factor $S(E, \Delta Q)$, summed over Q = 0.3–2.1 Å^{-1}, for single-crystal cordierite (with $\mathbf{Q} \perp c$-axis), measured with E_i = 12 meV at different temperatures.

D. DFT calculations of cordierite

To gain further insight into the location and motion of the water molecules in cordierite, we made DFT calculations as described above. The resulting calculated equilibrium configuration for the crystal structure of cordierite is shown in Fig. 12. The water molecule occupies a position close to the center of the cordierite

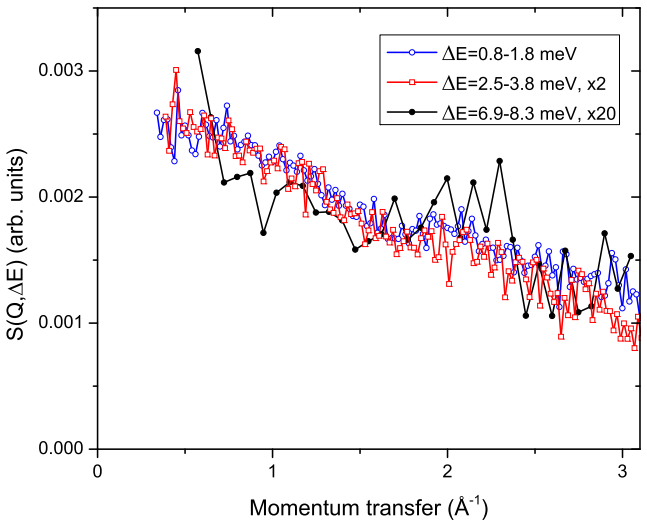

FIG. 9. Momentum-transfer dependences of the dynamical structure factor for different excitations at selected energies ΔE for dehydrated cordierite at T = 6 K.

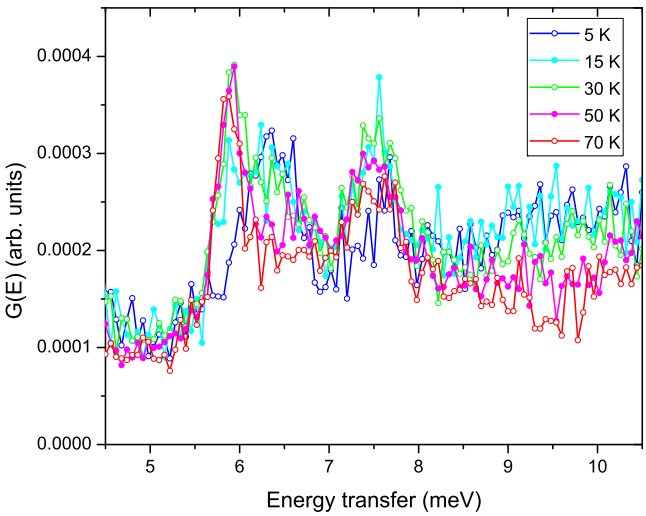

FIG. 11. The generalized vibrational density-of-states $G(E)$, summed over Q = 0.3–2.1 Å^{-1}, for single-crystal cordierite (with $\mathbf{Q} \perp c$-axis) and powdered dehydrated cordierite, measured with E_i = 12 meV at different temperatures.

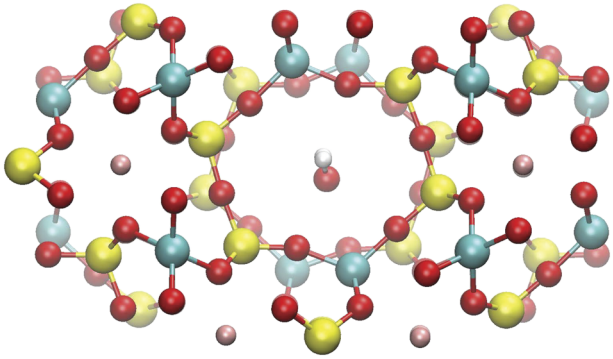

FIG. 12. Position of a water molecule in the channel of cordierite obtained by DFT calculations (projection on *ab*-plane, red—oxygen, blue—aluminum, yellow—silicon, pink—magnesium; the water molecule is in the center, red—oxygen, gray—hydrogen).

channel, with the molecule's center mass shifted slightly off center. The H-H axis is almost aligned with the *c*-axis of the cordierite crystal, and the dipole moment is directed along the *b*-axis. Due to the symmetry of the cordierite structure, water can occupy two possible positions (with the dipole moment up or down in Fig. 12), pointing at the narrower part of the channel toward the Al-tetrahedra. The calculated potential for the water molecule in cordierite (with the positions of the cordierite atoms fixed) as a function of water rotation around an axis parallel to the *c*-axis going through the center of mass of the water molecule is shown in Fig. 13 (curve 1). The

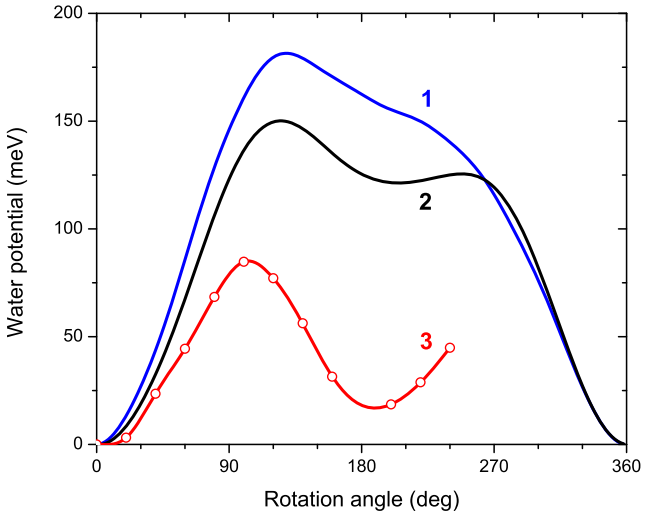

FIG. 13. Calculated potential of the water molecule in cordierite as a function of its rotation around an axis parallel to the *c*-axis of the crystal going through the center of mass of the water and the system is relaxed at the start (curve 1); curve 2 shows the potential in which the water molecule is fixed at the center of the channel, and the rotation axis goes through the water oxygen; and curve 3 displays the potential of the water (points) as a function of its rotation around an axis going through the center of the channel with all cage atoms relaxed at each rotation angle (the line is an interpolation with natural cubic spline).

system is relaxed at the start, but due to a shift in the position of the water molecule in the channel, the rotation results in nonrelaxed configurations and shows only a kink at 180°, instead of a second minimum similar to that in the starting configuration (0°). Translating the water molecule from the starting (relaxed) position to the center of the channel results in a slight increase in the total energy of the system, but the potential as a function of water rotation shows a deeper minimum at 180° (curve 2). Finally, we have calculated the potential by rotation of a water molecule around an axis going through the center of the channel with the positions of the cordierite atoms relaxed at each rotation angle (curve 3). The calculated potentials are useful for estimating the height of the energy barrier for water rotation between its two equilibrium positions in the channel. The results suggest that the true barrier height is probably around 100 meV. This value is comparable to the calculated equilibrium barrier height for water rotation around the *c*-axis in beryl,[10] but because of the reduced symmetry and preference for H_2O to align with the Al in the cordierite structure, the distance between the equivalent positions for the water protons in cordierite is about three times as large as that in beryl and, as a result, water in cordierite does not show any evidence of tunneling splitting of the ground state observed in beryl, at least at the energies probed in the current INS experiments, where the best energy resolution around elastic line was ~0.2 meV).

IV. CONCLUSIONS

We have shown that the dynamics of water in hydrophobic confinement of beryl and cordierite is very sensitive to even small changes in the structure of the confining cage. Applying a pressure of 22 kbar to beryl with type-I water results in a shift in the tunneling and low-energy vibrational peaks by ~2.5%, while the interatomic distances in beryl change by ~0.5%.

The INS study of type-II water in beryl, in which the H-H axis of the water molecule is in the *ab*-plane (it is parallel to the *c*-axis for type-I water), shows that its intramolecular vibrations are similar to those in type-I water in beryl, but its intermolecular vibrations are slightly different, and there is no evidence for the presence of tunneling peaks in the type-II water spectra.

The dynamics of type-I water in cordierite in the range of intramolecular modes is also similar to that for water in beryl. However, at low energies, it shows significantly different behavior, an absence of tunneling peaks, and abnormal behavior of the translational peak at ~6 meV, indicating a possible phase transition at about 20 K.

Thus, we have shown that small changes in the structure of hydrophobic confining cages cause large changes in water dynamics at low energies.

ACKNOWLEDGMENTS

The neutron-scattering research at the Spallation Neutron Source, Oak Ridge National Laboratory, was sponsored by the Scientific User Facilities Division, Office of Basic Energy Sciences, U.S. Department of Energy. ORNL is managed by UT-Battelle, LLC, under Contract No. DE-AC05-00OR22725 with the U.S. Department of Energy. This material is based upon work supported by the U.S. Department of Energy, Office of Science, Office of Basic

Energy Sciences, Chemical Sciences, Geosciences, and Biosciences Division. F.C.H. was supported by a Discovery Grant from the Natural Sciences and Engineering Research Council of Canada. The U.S. Government retains, and the publisher, by accepting the article for publication, acknowledges that the U.S. Government retains a nonexclusive, paid-up, irrevocable, worldwide license to publish or reproduce the published form of this manuscript, or allow others to do so, for U.S. Government purposes. The Department of Energy will provide public access to these results of federally sponsored research in accordance with the DOE Public Access Plan (http://energy.gov/downloads/doepublic-access-plan).

REFERENCES

[1]C. Beduz, M. Carravetta, J. Y.-C. Chen, M. Concistrè, M. Denning, M. Frunzi, A. J. Horsewill, O. G. Johannessen, R. Lawler, X. Lei, M. H. Levitt, Y. Li, S. Mamone, Y. Murata, U. Nagel, T. Nishida, J. Ollivier, S. Rols, T. Rõõm, R. Sarkar, N. J. Turro, and Y. Yang, Proc. Natl. Acad. Sci. U. S. A. **109**, 12894 (2012).
[2]K. S. K. Goh, M. Jiménez-Ruiz, M. R. Johnson, S. Rols, J. Ollivier, M. S. Denning, S. Mamone, M. H. Levitt, X. Lei, Y. Li, N. J. Turro, Y. Muratae, and A. J. Horsewill, Phys. Chem. Chem. Phys. **16**, 21330 (2014).
[3]A. I. Kolesnikov, J.-M. Zanotti, C.-K. Loong, P. Thiyagarajan, A. P. Moravsky, R. O. Loutfy, and C. J. Burnham, Phys. Rev. Lett. **93**, 035503 (2004).
[4]A. I. Kolesnikov, C.-K. Loong, N. R. de Souza, C. J. Burnham, and A. P. Moravsky, Physica B **385-386**, 272 (2006).
[5]L. M. Anovitz, E. Mamontov, P. ben Ishai, and A. I. Kolesnikov, Phys. Rev. E **88**, 052306 (2013).
[6]A. I. Kolesnikov, L. M. Anovitz, E. Mamontov, A. Podlesnyak, and G. Ehlers, J. Phys. Chem. B **118**, 13414 (2014).
[7]A. I. Kolesnikov, G. F. Reiter, T. R. Prisk, M. Krzystyniak, G. Romanelli, D. J. Wesolowski, and L. M. Anovitz, J. Phys.: Conf. Ser. **1055**, 012002 (2018).
[8]G. Diego Gatta, F. Nestola, G. D. Bromley, and S. Mattauch, Am. Mineral. **91**, 29 (2006).
[9]T. Armbruster, Phys. Chem. Miner. **12**, 233 (1985).
[10]A. I. Kolesnikov, G. F. Reiter, N. Choudhury, T. R. Prisk, E. Mamontov, A. Podlesnyak, G. Ehlers, A. Seel, D. J. Wesolowski, and L. M. Anovitz, Phys. Rev. Lett. **116**, 167802 (2016).
[11]B. P. Gorshunov, E. S. Zhukova, V. I. Torgashev, V. V. Lebedev, G. S. Shakurov, R. K. Kremer, E. V. Pestrjakov, V. G. Thomas, D. A. Fursenko, and M. Dressel, J. Phys. Chem. Lett. **4**, 2015 (2013).
[12]B. P. Gorshunov, E. S. Zhukova, V. I. Torgashev, E. A. Motovilova, V. V. Lebedev, A. S. Prokhorov, G. S. Shakurov, R. K. Kremer, V. V. Uskov, E. V. Pestrjakov, V. G. Thomas, D. A. Fursenko, C. Kadlec, F. Kadlec, and M. Dressel, Phase Transitions **87**, 966 (2014).
[13]E. S. Zhukova, V. I. Torgashev, B. P. Gorshunov, V. V. Lebedev, G. S. Shakurov, R. K. Kremer, E. V. Pestrjakov, V. G. Thomas, D. A. Fursenko, A. S. Prokhorov, and M. Dressel, J. Chem. Phys. **140**, 224317 (2014).
[14]P. Černy and F. M. Simpson, Can. Mineral. **15**, 489 (1977).
[15]A. Podlesnyak, M. Loguillo, G. M. Rucker, B. Haberl, R. Boehler, G. Ehlers, L. L. Daemen, D. Armitage, M. D. Frontzek, and M. Lumsden, High Pressure Res. **38**, 482 (2018).
[16]G. E. Granroth, A. I. Kolesnikov, T. E. Sherline, J. P. Clancy, K. A. Ross, J. P. C. Ru, B. D. Gaulin, and S. E. Nagler, J. Phys.: Conf. Ser. **251**, 012058 (2010).
[17]M. B. Stone, J. L. Niedziela, D. L. Abernathy, L. DeBeer-Schmitt, G. Ehlers, I. Garlea, G. E. Granroth, M. Graves-Brook, A. I. Kolesnikov, A. A. Podlesnyak, and B. Winn, Rev. Sci. Instrum. **85**, 045113 (2014).
[18]G. Ehlers, A. A. Podlesnyak, J. L. Niedziela, E. B. Iverson, and P. E. Sokol, Rev. Sci. Instrum. **82**, 085108 (2011).
[19]G. Ehlers, A. A. Podlesnyak, and A. I. Kolesnikov, Rev. Sci. Instrum. **87**, 093902 (2016).
[20]O. Arnold, J. C. Bilheux, J. M. Borreguero, A. Buts, S. I. Campbell, L. Chapon, M. Doucet, N. Draper, R. F. Leal, M. A. Gigg, and V. E. Lynch, Nucl. Instrum. Methods Phys. Res., Sect. A **764**, 156 (2014).
[21]R. T. Azuah, L. R. Kneller, Y. Qiu, P. L. Tregenna-Piggott, C. M. Brown, J. R. Copley, and R. M. Dimeo, J. Res. Natl. Inst. Stand. Technol. **114**, 341 (2009).
[22]S. W. Lovesey, *Theory of Neutron Scattering from Condensed Matter*, Nuclear Scattering Vol. 1 (Clarendon Press, Oxford, 1984).
[23]V. S. Oskotskii, Sov. Phys. Solid State **9**, 420 (1967).
[24]V. F. Sears, Neutron News **3**, 26 (1992).
[25]J. VandeVondele, M. Krack, F. Mohamed, M. Parrinello, T. Chassaing, and J. Hutter, Comput. Phys. Commun. **167**, 103 (2005).
[26]J. P. Perdew, K. Burke, and M. Ernzerhof, Phys. Rev. Lett. **77**, 3865 (1996).
[27]J. VandeVondele and J. Hutter, J. Chem. Phys. **127**, 114105 (2007).
[28]S. Goedecker, M. Teter, and J. Hutter, Phys. Rev. B **54**, 1703 (1996).
[29]D. Fan, J. Xu, Y. Kuang, ·X. Li, Y. Li, and H. Xie, Phys. Chem. Miner. **42**, 529 (2015).
[30]L. D. Landau and E. M. Lifshitz, *Quantum Mechanics: Non-Relativistic Theory*, 2nd ed., A Course of Theoretical Physics Vol. 3 (Pergamon Press, Oxford, 1965), p. 176.
[31]A. I. Kolesnikov, A. Podlesnyak, R. A. Sadykov, V. E. Antonov, M. A. Kuzovnikov, G. Ehlers, and G. E. Granroth, Phys. Rev. B **94**, 134301 (2016).
[32]T. A. Bulbak and S. V. Shvedenkova, Geochem. Int. **49**, 391 (2011).
[33]B. Winkler, G. Coddens, and B. Hennion, Am. Mineral. **79**, 801 (1994).
[34]B. Winkler and B. Hennion, Phys. Chem. Miner. **21**, 539 (1994).